AGU PUBLICATIONS

JGR

Journal of Geophysical Research: Space Physics

RESEARCH ARTICLE
10.1002/2016JA023007

Key Points:
- On 11 January 2014 Jupiter's UV aurora exhibits a superrotating polar spot: Signature of tail reconnection
- Concurrent bright, broad main emission results from enhanced flow shears around reconnection inflows
- Large equatorward emissions are signatures of hot plasma injections from earlier reconnection inflow

Supporting Information:
- Supporting Information S1
- Movie S1

Correspondence to:
R. L. Gray,
r.gray@lancaster.ac.uk

Citation:
Gray, R. L., S. V. Badman, B. Bonfond, T. Kimura, H. Misawa, J. D. Nichols, M. F. Vogt, and L. C. Ray (2016), Auroral evidence of radial transport at Jupiter during January 2014, *J. Geophys. Res. Space Physics*, *121*, doi:10.1002/2016JA023007.

Received 27 MAY 2016
Accepted 20 SEP 2016
Accepted article online 24 SEP 2016

Auroral evidence of radial transport at Jupiter during January 2014

R. L. Gray[1], S. V. Badman[1], B. Bonfond[2], T. Kimura[3], H. Misawa[4], J. D. Nichols[5], M. F. Vogt[6], and L. C. Ray[7]

[1]Department of Physics, Lancaster University, Lancaster, UK, [2]Space Sciences, Technologies and Astrophysics (STAR) Institute, Université de Liège, Liège, Belgium, [3]High Energy Astrophysics Laboratory, RIKEN, Wako, Japan, [4]Planetary Plasma and Atmospheric Research Center, Tohoku University, Sendai, Japan, [5]Department of Physics and Astronomy, University of Leicester, Leicester, UK, [6]Center for Space Physics, Boston University, Boston, Massachusetts, USA, [7]Mullard Space Science Laboratory, University College London, London, UK

Abstract We present Jovian auroral observations from the 2014 January Hubble Space Telescope (HST) campaign and investigate the auroral signatures of radial transport in the magnetosphere alongside contemporaneous radio and Hisaki EUV data. HST FUV auroral observations on day 11 show, for the first time, a significantly superrotating polar spot poleward of the main emission on the dawnside. The spot transitions from the polar to main emission region in the presence of a locally broad, bright dawnside main emission feature and two large equatorward emission features. Such a configuration of the main emission region is also unreported to date. We interpret the signatures as part of a sequence of inward radial transport processes. Hot plasma inflows from tail reconnection are thought to flow planetward and could generate the superrotating spot. The main emission feature could be the result of flow shears from prior hot inflows. Equatorward emissions are observed. These are evidence of hot plasma injections in the inner magnetosphere. The images are thought to be part of a prolonged period of reconnection. Radio emissions measured by Wind suggest that hectometric (HOM) and non-Io decametric (DAM) signatures are associated with the sequence of auroral signatures, which implies a global magnetospheric disturbance. The reconnection and injection interval can continue for several hours.

1. Introduction

Iogenic plasma generated in the inner magnetosphere is transported radially outward through a quasi steady state process to the outer magnetosphere where it is lost down the magnetotail. At Earth, auroral features have been shown to be a manifestation of magnetospheric transport processes. Therefore, it is reasonable to assume that also Jupiter's far ultraviolet (FUV) aurora provides a global view of events occurring through the Jovian magnetosphere. Auroral features are measured in system III (λ_{III}), a jovicentric longitude-latitude grid which corotates with the planet with a period of 9.925 h, as defined in *Dessler* [1983].

In the middle magnetosphere (15–40 R_J), the angular speed of Iogenic plasma falls as it is centrifugally driven outward. A field-aligned current system that closes through radial currents in the equator is responsible for transferring angular momentum in order to maintain partial corotation. The upward current produces Jupiter's auroral main emission [*Hill*, 2001; *Cowley and Bunce*, 2001]. Its primary variability corresponds to changes in mass loading and mass outflow rate in the middle magnetospheric "corotation breakdown region" [*Nichols*, 2011; *Ray et al.*, 2012].

In the outer magnetosphere (>40 R_J), the magnetic field is stretched to the point of collapse and field reconnection [*Vasyliunas*, 1983]. Reconnection results in planetward flows of very hot, tenuous plasma and tailward flows as Iogenic plasma is ejected from the system [*Kronberg et al.*, 2005; *Vogt et al.*, 2010]. Small auroral spots, known as polar spots, have been detected poleward of the main oval on the dawnside and on the nightside. They are associated with the planetward flow of dipolarized magnetic field lines following reconnection in the magnetotail [*Grodent et al.*, 2004; *Radioti et al.*, 2008, 2010, 2011; *Ge et al.*, 2010]. The spots are reported to corotate, and their size is typically a few degrees in longitude and a degree in latitude in the ionosphere [*Radioti et al.*, 2008].

In the inner magnetosphere (<15 R_J), the process of interchange occurs as regions of hot, tenuous plasma are encountered by outflowing cold, dense Iogenic plasma. The tenuous and dense plasma interchange position in order to conserve magnetic flux. Narrow interchange fingers have been detected in the vicinity of Io [*Kivelson et al.*, 1997; *Thorne et al.*, 1997]. Injections of hot plasma have been detected at 9–27 R_J radial distance, extending up to ~1 R_J in azimuth [*Mauk et al.*, 1999, 2002]. The auroral signatures of hot plasma injections have also been detected as diffuse patches of aurora at the corresponding latitudes equatorward of the main auroral oval [*Mauk et al.*, 2002; *Dumont et al.*, 2014]. The auroral features can be driven either by scattering of electrons into the loss cone or by field-aligned currents associated with pressure gradients within and at the boundaries of the hot plasma. These injections play a role in conserving magnetic flux; *Dumont et al.* [2014] estimated that they can account for at least 18 % of the inward flux required to balance the Iogenic outflow.

Wave-particle interactions in the region 10–17 R_J are thought to scatter electrons into a field-aligned distribution, leading to a transition region at these distances where the electron pitch-angle distribution (PAD) changes and to a secondary auroral oval sometimes visible at lower latitudes than the main oval [*Grodent et al.*, 2003; *A. Tomás et al.*, 2004; *A. T. Tomás et al.*, 2004; *Radioti et al.*, 2009].

The most equatorward auroral features are the moon footprints [*Bonfond*, 2012]. Because of their known radial position in the magnetosphere, they are used to validate mapping along magnetic field lines between magnetospheric source regions and the ionospheric auroral signatures.

Finally, poleward auroral signatures have been linked to solar wind interaction at the dayside magnetopause [*Pallier and Prangé*, 2001; *Gladstone et al.*, 2002; *Vogt et al.*, 2011].

Considering how the outer and inner magnetospheric processes are linked, studies of Saturn's magnetospheric dynamics have revealed the presence of a plasmapause at the boundary of the nightside internally driven reconnection inflow and dense inner magnetospheric plasma [*Thomsen et al.*, 2015]. Evidence of interchange across the sharp boundary was detected in both hot, planetward plasma and cool, tailward plasma. *Mitchell et al.* [2015] have also suggested that inward flows from reconnection could trigger interchange processes in the inner magnetosphere. A similar boundary could be present in Jupiter's magnetosphere at the outer edge of the dense, cold plasma torus. However, while reconnection and therefore its inflows in the outer magnetosphere are expected to occur preferentially on the dawnside [*Vogt et al.*, 2010, 2014], statistical studies of the inner magnetospheric injections and their auroral signatures show no local time preference [*Mauk et al.*, 1999; *Dumont et al.*, 2014].

The 2014 Hubble Space Telescope (HST) campaign has been studied previously. We take into account the relevant work in our study. *Kimura et al.* [2015] have suggested that transient brightening events during the observational interval are driven by internal processes, not externally by the solar wind. *Yoneda et al.* [2015] have shown that there was no increase in sodium nebula brightness, indicating that Io was not significantly volcanically active before the campaign. S and O emissions in the inner Io torus are observed to be steady over the observation interval [*Tsuchiya et al.*, 2015]. It is therefore unlikely that the transient brightening is due to increased Iogenic outflow. This study further investigates the brightening event on day 11.

In this paper, we present auroral observations of a superrotating polar spot transition from the polar to main emission region in the presence of a broad, bright main emission feature and two large equatorward emission features. The magnetospheric processes that cause these auroras occur at different radial distances. We therefore investigate the signatures as part of a sequence of inward radial transport processes.

2. Overview of Observations and Data Reduction

The Hubble Space Telescope (HST) Space Telescope Imaging Spectrograph (STIS) with the SrF2 filter was used to capture "time tag" images of Jupiter's FUV northern aurora between days of year 1 to 16 of 2014. These emissions mainly consist of H Lyman alpha and H_2 Lyman and Werner bands. The band pass of the SrF2 filter is 1250–1900 Å, i.e., it rejects light at shorter wavelengths including the H Lyman alpha line at 1215 Å. There is on average one HST "visit" per day, with exceptions of day 11 and day 13 having two and three visits, respectively. Each ~45 min long visit consists of two sequences of 700 s time tag imaging sequences interrupted by a 200 s spectral observation. The imaging observations are split into seven images with 100 s exposures.

The images were processed through the Boston University pipeline [*Nichols et al.*, 2009; *Clarke et al.*, 2009], correcting for dark current, flat field, and geometric distortion. The counts were converted to kiloRayleighs

emitted from H_2 over the wavelength range 700–1800 Å, assuming a color ratio of 2.5 [*Gustin et al.*, 2012]. The images were projected onto a planetocentric longitude-latitude grid assuming a peak auroral emission height of 240 km above the 1 bar pressure level of an oblate spheroid [*Vasavada et al.*, 1999]. The resolution of the projected image is 0.25° × 0.25 °. Further details about data reduction and projection accuracy can be found in *Nichols et al.* [2009] and *Grodent et al.* [2003], respectively.

3. Results

3.1. Auroral Features

Figure 1 shows six 100 s exposure images taken on 11 January 2014. The images are clipped at ∼2° below the planetary limb to avoid analysis where there are significant inaccuracies due to the oblique viewpoint [*Grodent et al.*, 2003]; the field of view is bounded by the dashed white line. The main emission boundary (shown in Figure 1f) is defined as a strip that is 1° poleward and 2° equatorward of the average main emission for the 2014 HST campaign. Given the variable main emission morphology through the campaign, the strip sometimes cuts off the extreme edges. The polar region is defined as poleward of the main emission and the equatorward region is equatorward of the main emission, up to ∼1.5° poleward of the Io footprint [*Hess et al.*, 2011]. A video showing all the images from day 11 is included in the supporting information.

In the first sequence of the first visit (00:31–00:41 UT, Figure 1a), three features are highlighted; feature B is a section of the main emission and C and D are both large equatorward emission features. In the second sequence of the first visit (01:01–01:11 UT, Figures 1b–1e), feature A is a polar spot. This is circled in Figure 1b. The images, which are shown fixed in SIII longitude with λ_{III}=180 ° at the bottom, indicate that the polar spot is superrotating, i.e., moving faster than the features that are fixed in λ_{III}.

The spot center (the brightest central point of the 200 kR contour) moves ∼ 8° (∼8000 km) in the ionosphere over the 10 min sequence, corresponding to ∼270% corotation speed (including both azimuthal and radial motion, where 100% corresponds to corotation). The spot is up to 4° wide in longitude and 1° in latitude and brightens to an average of ∼300 kR. It is separated from the campaign average main emission position initially by 3.8° and moves equatorward to a separation of 2° latitude over the 10 min sequence. The spot extends between 200 and 211° longitude over all images. The spot appears on the dawn flank, similar to those reported in *Radioti et al.* [2008, 2010], which were interpreted as a signature of reconnection in the magnetotail.

The main emission is usually broad at dusk and well defined/narrow at dawn [*Gustin et al.*, 2006]. However, in this visit (00:33–01:11 UT), in the region λ_{III} ∼185–200° the main emission appears notably expanded in latitude (up to ∼ 2.5° latitude either side of the average campaign main emission position) compared to the rest of the campaign and previous observations. This unusual feature could be due to a structure superposed on the main emission or an expansion of the emission itself. Figure 2 shows the substructure of feature B at 00:41 UT. The substructure consists two extremely bright regions (up to >6.8 MR) which appear to subcorotate over the sequence. The broadness of the feature is obvious when compared to the main emission on the opposite side of the oval, between λ_{III} ∼150 and 160°. The main emission region at B is also very bright; the power in the total main emission region in these images is consistently over 1000 GW, compared to typical power of ∼500 GW over the rest of the 2014 campaign.

The observed morphology is reminiscent of but distinct from the "dawn storm" events described by *Gustin et al.* [2006] and *Nichols et al.* [2009], in which the entire dawn length of the main emission is brightened and broadened. The brightness of the dawn storm morphologies has been reported to peak at 1.8 MR [*Gustin et al.*, 2006]. The peak brightness of the main emission feature B is >6.8 MR. Feature B is also distinct from the multiple dawn arcs reported by *Grodent et al.* [2003].

The last image of this sequence (shown in Figure 1e) shows the superrotating spot entering the area of bright and expanded main emission ∼ 200° λ_{III}. This implies that the field lines mapping to the spot are in the vicinity of the dawn sector corotation breakdown region, which leads to the main emission [*Cowley and Bunce*, 2001; *Vogt et al.*, 2011, 2015]. The breadth of the main emission has reduced to the steady state configuration (although dimmer, up to ∼400 kR) by the next HST visit at 19:39 UT (shown in Figure 1f).

There are two large equatorward emissions at 154–169° (emission C) and 133–152° (emission D). Emission C has bright patches of up to 1600 kR and extends into the main emission oval. Emission D is more diffuse, reaching a peak brightness of only 600 kR, and is centered at lower latitudes, extending to within 2° of the Io Footprint (IFP) contour. The average brightness in emission D is 270 kR. These emissions are present at the

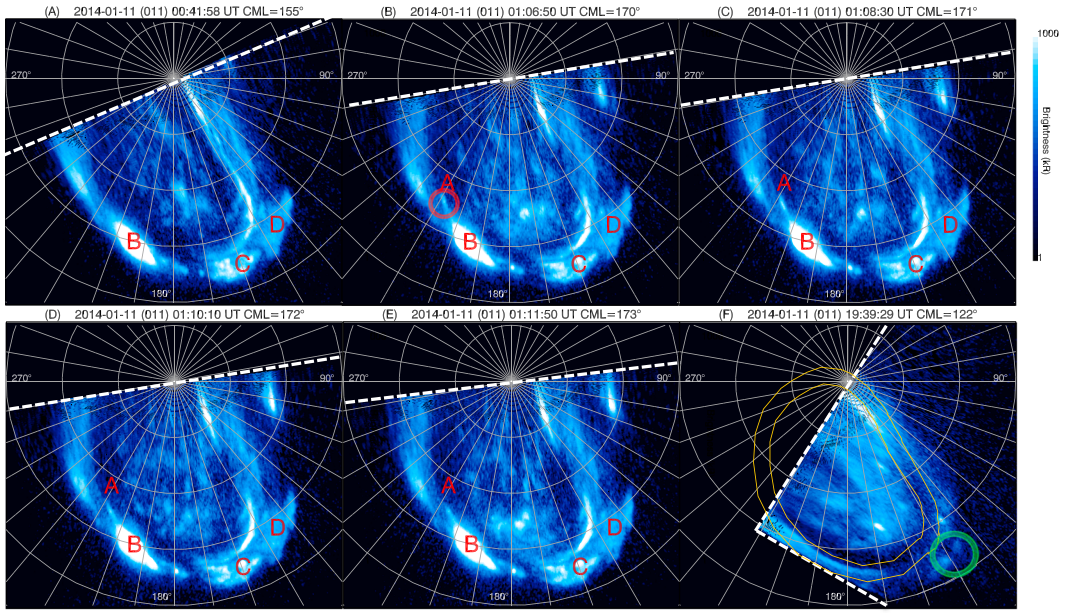

Figure 1. Six panels showing polar-projected HST image of Jupiter's northern FUV aurora on 11 January 2014 at (a) 00:41 UT, (b) 01:06 UT, (c) 01:08 UT, (d) 01:10 UT, (e) 01:11 UT, and (f) 19:39 UT. For each image the exposure time was 100 s. The Central Meridian Longitude (CML) is shown. The image is displayed with a log intensity scale saturated at 1000 kR. The dashed white line shows the edge of the field of view. The grey lines indicate a 10° × 10° jovicentric latitude-system III longitude grid. The image is oriented such that 180° λ_{III} is directed toward the bottom and λ_{III} labels are displayed in grey. In Figures 1a–1e, labels indicate the superrotating polar spot (A), circled in Figure 1b, a bright and expanded main emission region (B) and two equatorward emissions (C and D). The yellow lines in Figure 1f, taken ~18 h after the first visit, show the boundaries of the main emission region, derived from the average main emission position over the 2014 campaign. The poleward region of the main emission strip is the "polar region" and the equatorward region up to 1.5 ° poleward of the Io footprint is the "equatorward" region. Equatorward emissions circled in green on this image are possible remnants of the equatorward features C and D.

beginning of this HST sequence (00:31–00:41 UT, Figure 1a), so their generation must have occurred before the transit of the polar spot into the main emission region.

The longevity of the equatorward emissions is also comparable to that described by *Dumont et al.* [2014]; the consecutive HST sequences starting at 00:31 UT and 01:01 UT both show the emissions. There are faint

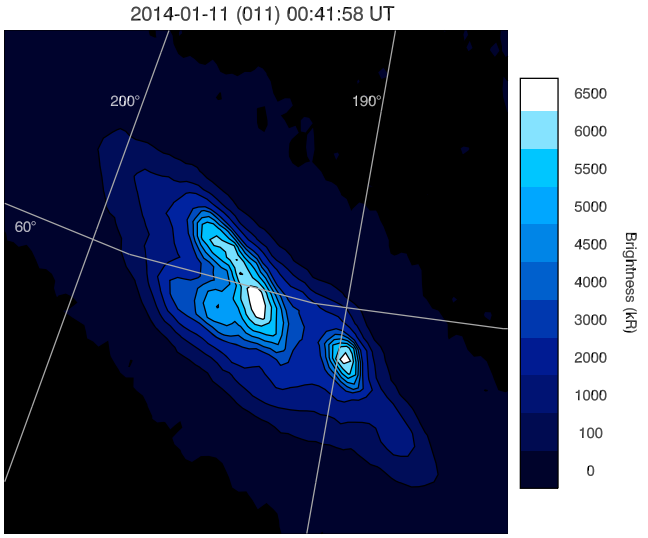

Figure 2. Polar-projected HST image of feature B taken at 00:41 UT, as in Figure 1a, showing substructure. Longitude and latitude labels are displayed.

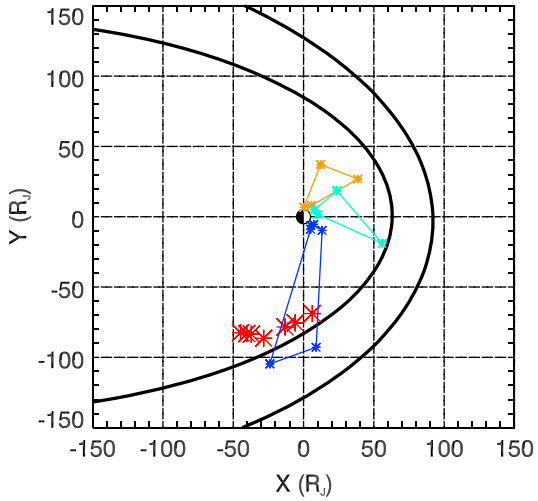

Figure 3. The location in the equatorial plane of the auroral features observed on 11 January 2014. The red stars show the equatorial mapping of the center (specifically the brightest central point of the 200 kR contour) of the superrotating polar spot as it moves over the image sequence and the colored boxes are the extrema of the auroral features. The poleward edges of the features were mapped using the flux equivalence method at 170° CML [*Vogt et al.*, 2011, 2015] with the GAM internal field model [*Grodent et al.*, 2008]. The VIPAL internal field model alone was used to map the equatorward edges of the main emission and equatorward emission features [*Hess et al.*, 2011]. The Sun is to the right-hand side. The blue box shows the expanded main emission (B), the green shows the left-hand equatorward feature (C), and the orange shows the right-hand equatorward feature (D). Solid black lines indicate the compressed and expanded magnetopause after *Joy et al.* [2002].

structures on images taken at 19:39 UT (second visit, Figure 1f, circled green) at the same longitudes as feature C in the previous visit. The faint structures could be a remnant of feature C, which would give a minimum lifetime for this equatorward emission of 18.5 h.

3.2. Magnetospheric Source Regions

In order to investigate the potential magnetospheric source region of the auroral features, we map field lines from the Northern Hemisphere to the equatorial magnetosphere using the Grodent Anomaly Model (GAM) and the VIPAL model. The VIPAL model is an update to the VIP4 internal magnetic field model and is based on Voyager and Pioneer magnetic field measurements, modeling of the lowest orders of the magnetic anomaly, and corrects for the longitudinal position of the magnetic field lines mapping to Io's orbit. Figure 3 shows the mapped location of the center of the superrotating spot (specifically the brightest central point within the 200 kR contour), in the equatorial plane of the magnetosphere alongside the mapped source regions of the extrema of the main emission and two equatorward emissions shown in Figure 1. The red stars show the equatorial mapping of the center of the superrotating polar spot and the boxes the extrema of the other auroral features. The magnetopause is indicated by the solid black lines and shows both the compressed and the expanded configurations after *Joy et al.* [2002].

The poleward edges of the features were mapped using the flux equivalence method at 170° CML [*Vogt et al.*, 2011, 2015]. The flux equivalence method requires a choice of internal field model. The spot and poleward edges of the main emission use the GAM internal field model because it provides the most accurate match to the Ganymede footprint at these longitudes [*Grodent et al.*, 2008; *Vogt et al.*, 2015]. Out of the internal field models available, GAM predicts the most tailward source for the spot and main emission, which is consistent with the initial notable high latitude of the spot and the interpretation of polar spots as a result of tail reconnection. For consistency, the GAM model of the internal field was used for the poleward edges of the equatorward emission [*Vogt et al.*, 2011, 2015]. The flux equivalence method is used for $>15\ R_J$ where currents can cause field stretching. The VIPAL internal field model alone was used to map the equatorward edges of the main emission and equatorward emission features [*Hess et al.*, 2011].

As the polar spot superrotates around the planet, its mapped radial distance from the planetary center decreases from 95 to $\sim$70 R_J as it moves from 0400 to 0615 LT. These radial distances are consistent with the locations of reconnection events observed in situ with Galileo [*Kronberg et al.*, 2005] and the statistical X line in this sector [*Vogt et al.*, 2010]. Figures 1b–1e show that the spot (A) moves closer to the enhanced main

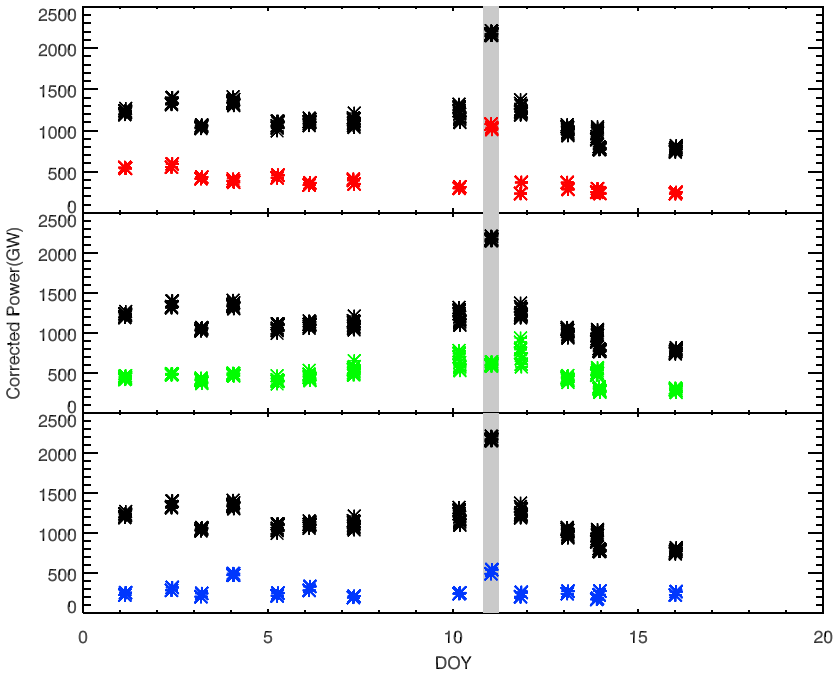

Figure 4. Power emitted from the different auroral regions over the 2014 HST campaign. The regions shown in color from top to bottom are the main emission region (red), polar region (green) and the equatorward region (blue). The vertical grey shaded region indicates the HST visits of interest at 01:00 UT on day 11. The boundaries of these regions are indicated in Figure 1f. In each plot, the black points indicate the total power in order to indicate the contribution of each region to the total power. The power has been corrected for viewing geometry variation after [*Nichols et al.*, 2009].

emission region (B). Correspondingly, the map in the equatorial plane (Figure 3) shows that the final mapped source region of the spot and the main emission source region are colocated. The total distance between the first and last mapped location of the spot is ~56 R_J. This corresponds to an average propagation speed of 6450 km/s in the magnetosphere over the 10 min sequence.

The mapped main emission region (feature B, blue outline) extends from 8 R_J to as far as ~110 R_J from the planet. The majority of points within this feature, however, map to within 15–45 R_J, which is consistent with the modeled corotation breakdown region of 15–30 R_J [*Vogt et al.*, 2015] in the dawn sector. The source region maps to between 0500 and 0915 LT.

The brighter equatorward emission source region (feature C, green outline) is farther from the planet than the second equatorward emission source region (feature D, orange outline). The source region of emission C extends over ~8–58 R_J and between 1100 and 1500 LT. The source region of emission D extends over ~6–45 R_J and between 1445 and 1730 LT.

3.3. Emitted Auroral Powers

Comparison of the power emitted by each region of the aurora over time can be used to indicate how energy is moved through the magnetosphere. The power emitted from each region can be extracted from the images following the procedure outlined in *Gustin et al.* [2012].

The observed auroral power is dependent on the CML. For some viewing geometries, a significant fraction of the auroral emission is located behind the planetary limb because of the magnetic dipole tilt of 10°. Following the procedure outlined in *Clarke et al.* [1980] and more recently *Nichols et al.* [2009] and *Bonfond et al.* [2012], the corrected UV power in each region of the aurora was extracted from the HST images.

Figure 4 shows the time series of the power in each region of the aurora. The day 11 event dominates the time series. The total auroral power peaks at ~2200 GW. Comparison of the contributions of each auroral region and the morphologies themselves (see Figure 1) show that main emission brightness region is the primary contributor to the power (~1100 GW) and that the breadth of feature B causes the power to "leak" over the defined regional boundaries into the other regions. There is additionally a significant contribution from the large equatorward emissions (~540 GW). These are similar to the observed power of equatorward emissions

observed by *Bonfond et al.* [2012]. The contribution of the two large equatorward emissions C and D alone is ~390 GW. The superrotating polar spot does not contribute notably to power in the polar region because of its small size.

The next HST image (19:39 UT, Figure 1f) was taken 18.5 h after the image sequence showing the above features (01:01–01:11 UT, Figures 1b–1e). The total auroral power decreased from ~2200 GW at 01:11 UT back to ~1300 GW at 19:39 UT on day 11. Using a simultaneous data set from the Hisaki satellite, which measures extreme ultraviolet (EUV) power emitted from the whole northern polar region quasi-continuously, the time interval during which the power was elevated above average values can be constrained to just 7 h [*Kimura et al.*, 2015]. The extremely bright main emission feature B and large equatorward emissions C and D are the primary contributors to the power. The long-term variations in power are discussed by *Badman et al.* [2016].

4. Discussion: Interpretation of Auroral Signatures

Polar spots which are not superrotating have been interpreted as auroral signatures of magnetic reconnection [*Grodent et al.*, 2004; *Radioti et al.*, 2008, 2010]. The superrotating polar spot (A) is also interpreted as the auroral response of magnetic field reconnection in the magnetotail because of its similar size, direction of motion, and location. The superrotating spot appears at higher latitude relative to the main emission compared to the other polar spots seen in this campaign, such as on day 4 (not shown here). The typical separation of these spots from the main emission is around 1° of latitude, consistent with observations of polar spots by *Radioti et al.* [2008]. However, on day 11, the spot is as far as 3.8° poleward of the campaign average main emission location. In general, more poleward emissions correspond to events farther from the planet, so this indicates that reconnection is occurring further from the planet (or at least farther from the corotation breakdown/main oval region) in the day 11 case than in other previously reported polar spot cases.

Two explanations of the unusual spot observations are presented. First, following *Nichols et al.* [2014], the site of magnetic reconnection itself propagates rapidly as flux over a large spatial region reconnects. As the field dipolarizes, Alfvén waves are launched from the reconnection site and generate an auroral signature. As the reconnection site moves, so does its ionospheric footprint. It is noted that the mapped location of the superrotating spot in the magnetosphere follows the location of the statistical Vasyliunas cycle X line in the magnetotail [*Vogt et al.*, 2010], i.e., moving closer to the planet with increasing LT. In this scenario, to match the observations the X line would need to propagate at ~6500 km/s.

Alternatively, hot tenuous plasma flowing very quickly planetward from a distant reconnection site can produce a signature at very high latitudes relative to the main emission and rotate around the planet at high azimuthal velocity. By analogy to auroral streamers at Earth, as the field line moves azimuthally and planetward around dawn, the foot point in the ionosphere is also expected to move [*Henderson et al.*, 1998; *Nakamura et al.*, 2001; *Nishimura et al.*, 2011]. The relatively fast contraction of the dipolarizing field line in the magnetosphere past the surrounding field lines causes a gradient in B_z and, therefore, a field-aligned current system [e.g., *Kasahara et al.*, 2011]. This has been observed at Earth by the Thermal Emission Imaging System (THEMIS) mission [*Keiling et al.*, 2009]. *Cowley et al.* [2015] showed that for a simple 1-D current sheet, a newly reconnected field line (dipolarization) will contract planetward with a speed equal to the difference between the Alfvén speed and the tailward flow of plasma on stretched nightside field lines. Taking the observed speed of the auroral spot, ~6500 km/s, as the speed of planetward contraction and an estimate of the downtail plasma flow as 350 km/s [*Krupp et al.*, 2004; *Cowley et al.*, 2015], the Alfvén speed (defined as $V_A = \frac{B}{\sqrt{2}\sqrt{\mu_0 n_i m_i}}$, where B is the magnetic field strength, μ_0 is the magnetic constant, n_i is the ion number density, and m_i is the ion mass) must be >6000 km/s. For a typical value of the field strength outside the current sheet of 7 nT (taken at 80 R_J) [*Kivelson and Khurana*, 2002], this requires a very low ion mass density (e.g., a proton density of 1×10^{-3} cc^{-1}), indicating that in this scenario, reconnection occurred in a low density region such as the lobe.

On day 11 (00:31–01:11 UT), the main emission is locally broadened and bright at emission B. The mapping of the path of the superrotating spot indicates reconnection inflows into this region. This implies that there are flows into the main emission region from reconnection events in the more distant magnetotail. Prior reconnection events may have caused similar flows. The resulting flow shears and dipolarized field lines generate field-aligned currents and enhanced auroral emission [*Kasahara et al.*, 2013; *Palmaerts et al.*, 2014], as indicated by the structure of feature B, shown in Figure 2. These effects could be compounded by an increase in ionospheric conductivity in the ionosphere locally to generate the bright signature observed. Increases in electron

precipitation can increase the ionospheric conductivity [*Nichols and Cowley*, 2004]. Models have shown that this can increase the coupling currents, generating bright and broadened aurora [*Nichols and Cowley*, 2003].

The main emission in feature B has returned to a normal configuration by the second visit of day 11 (Figure 1f). Assuming that a significant proportion of the total EUV power measured by Hisaki was from the large and exceptionally bright feature B, the lifetime of feature B may be constrained to just ~7 h. Feature B is interpreted as the result of enhanced flow shears, so it is suggested that enhanced inflow from the tail could also have continued for ~7 h.

Equatorward emissions have been linked to hot plasma injections [*Mauk et al.*, 2002; *Dumont et al.*, 2014; *Radioti et al.*, 2009; *Tomás et al.*, 2004; *Bonfond et al.*, 2012]. Emission regions C and D are unlike the morphologies described by *Dumont et al.* [2014], which are smaller and brighter. They are also larger than the emissions characterized by *Mauk et al.* [2002] as signatures of injections in the inner magnetosphere.

Similar features were identified in observations from 2007 with associated high powers in the equatorward region [*Nichols et al.*, 2009; *Bonfond et al.*, 2012]. These injections were attributed to increased Iogenic outflow during a volcanically active time. In particular, *Bonfond et al.* [2012] showed an increase in the occurrence rate of high power equatorward emission following increased Io activity compared to a prior period. Before the volcanically active period only 1 in 41 days showed high power emission, whereas after the activity the rate was 8 in 32 days. The occurrence rate in the 2014 campaign (which has a similar observational cadence to the 2007 campaign) is 3 in 16 days. This is similar to that observed in the period associated with Iogenic activity. However, in the present case, observations of the Io sodium nebula brightness [*Yoneda et al.*, 2015] and EUV power of the inner torus [*Tsuchiya et al.*, 2015] show no indication that Io volcanic activity has increased in the weeks prior to or during this observational interval. It is therefore suggested that inflow from reconnection causes hot plasma injections to generate the large signatures observed (analogously to bursty bulk flows at Earth), without requiring increased Iogenic outflow as in the 2007 case.

Following the discussion above, features C and D could have formed following reconnection-driven inflows in the preceding hours. Polar spots regularly appear in groups [*Grodent et al.*, 2004; *Radioti et al.*, 2008, 2010] and reconnection signatures in the tail can be clustered [*Vogt et al.*, 2014] implying reconnection events can happen in succession across field lines. There were no other polar spots observed during the 2 h of observations on this day; however, this may be expected given the low observational cadence. *Kasahara et al.* [2011] studied the effect of reconnection on the Jovian plasma sheet and found that during an extended interval of tail reconnection (up to 18 h) involving both closed and open field lines, a jet of electrons at the dipolarization front was detected traveling planetward at 7500–17000 km/s. This is similar to the velocity of the superrotating auroral spot inferred from the magnetic mapping (6450 km/s).

The equatorward emission D lies within the longitudinal range ($150° < \lambda_{III} < 210°$) and expected brightness (270 kR) identified for the secondary oval associated with the PAD boundary [*Grodent et al.*, 2003; *A. T. Tomás et al.*, 2004; *Radioti et al.*, 2009]. Enhancement of this feature can also be attributed to hot plasma injections since the hot population would enhance the waves responsible for the electron scattering [*A. Tomás et al.*, 2004; *Woodfield et al.*, 2013].

Previous observations show auroral signatures of injections can last over 34 h [*Bonfond et al.*, 2012]. Possible remnants of equatorward features C and D have been identified in HST observations made 18.5 h later (Figure 1f). This implies that the effects of hot plasma injections (e.g., further planetward transport and wave-particle interactions) can continue for 18.5 h.

In summary, the HST image auroral signatures have been interpreted as hot plasma inflows from tail reconnection (superrotating polar spot), flow shears in the dawnside middle magnetosphere (locally bright and broad dawnside main emission), and evidence of hot plasma injections in the inner magnetosphere (equatorward emission). It is not suggested that the magnetospheric counterpart of the superrotating spot causes the other features observed at the same time but that the superrotating polar spot signature is part of a prolonged reconnection interval.

Reconnection can proceed on open field lines if all the closed field lines have first been reconnected. The superrotating spot is seen at particularly high latitudes compared to previously reported spots, which are thought to have formed as part of the Vasyliunas cycle. Open field lines will map to more poleward emissions than the closed field lines and Dungey cycle reconnection is expected to take place in the far tail [*Badman and Cowley*, 2007]. It is suggested that the observed superrotating spot signature appears near the end of a

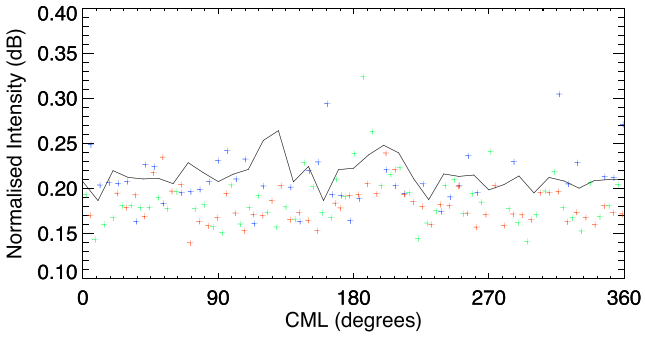

Figure 5. Averaged intensity at 3.5 MHz from Wind/WAVES sorted by CML for the planetary rotation before (blue, 15:10–01:00 UT), during (green, 01:00–11:10 UT), and after (red, 11:10–21:10 UT) the auroral sequence in Figures 1b–1e on day 11. The solid line shows campaign average intensity, in 10° bins. The colored points plot the intensity averaged over 10° bins for successive rotations.

prolonged reconnection interval, involving (Vasyliunas type) closed field line reconnection, possibly proceeding onto open field lines.

We now examine Jupiter's radio emissions for additional evidence of magnetospheric dynamics. *Louarn et al.* [2014] showed that inflows from tail reconnection were correlated (within one planetary rotation, ~10 h) with intensifications of the auroral hectometric radiation (HOM, 0.5 to few MHz) and the subsequent appearance of new narrowband kilometric radiation (nKOM, 40–150 kHz) sources in the outer Io plasma torus. Intensifications of non-Io decametric radiation (DAM, MHz) have been correlated with the arrival of solar wind shocks in some cases, although the physical process leading to the intensification has not been described [*Hess et al.*, 2014]. Increases in HOM emission have also been related to high solar wind dynamic pressure [*Gurnett et al.*, 2002].

Wind Radio and Plasma Waves (WAVES) data, recorded in Earth orbit at the L1 Lagrange point, were examined for this interval [*Bougeret et al.*, 1995]. There were many intense solar type III radio bursts during this campaign. These bursts extend over the full frequency range and have a characteristic shape in frequency-time space, wherein the frequency decreases with time. Although the data are heavily contaminated by solar bursts, it is possible to pick out other radio emission structures using both the spectra and analysis of the intensity as a function of Jupiter CML [e.g., *Yoneda et al.*, 2013].

Figure 5 shows the average intensity from days 1–16 at one frequency band (3.5 MHz), where HOM is expected, as a function of CML (black line). The occurrence probability of HOM is known to peak at CML around 30°, 120°, and 270° [*Galopeau and Boudjada*, 2005]. The peak at 120° indicates that the HOM was detected by Wind at this frequency during the interval despite the significant solar activity.

The blue, green, and red points in Figure 5 show the intensities at 3.5 MHz from the planetary rotations around the auroral image sequence shown in Figures 1b–1e at 01:01–01:11 UT. We show the rotations before and after the image sequence in order to show that the HOM signature observed is nonperiodic. The blue points show the planetary rotation before the auroral sequence; the green starts at the time of the auroral sequence and the red at the rotation after the sequence. The intensity of emission during the end of the first rotation (blue, 15:10–01:00 UT) and beginning of the middle rotation (green, 01:00–11:10 UT) around CML 150–220° exceeds the campaign average. The rotation after the image sequence (red, 11:10–21:10 UT) does not show significant intensity around the same CML, as expected for a signature that is nonperiodic. The majority of the points are lower intensity compared to the campaign average because there is lower type III burst activity at this frequency around day 11 compared to the rest of the campaign. The blue point at 310° CML above the campaign average has been checked against the frequency-time spectrogram and is not associated with HOM but is associated with a solar burst on day 10. The other HOM associated frequency bands were checked and CML 150–220° consistently showed increased intensity. Other points above the campaign average show variation across other frequency bands, so these are not HOM.

The raised intensity at HOM frequencies around the time of the HST images is also evident in Figure 6a, the frequency-time spectrogram, at 00:30–02:30 UT between 0.7 and 4 MHz. The emission frequency increases with time, opposite to the solar type III bursts also occurring. This potential HOM burst is detected

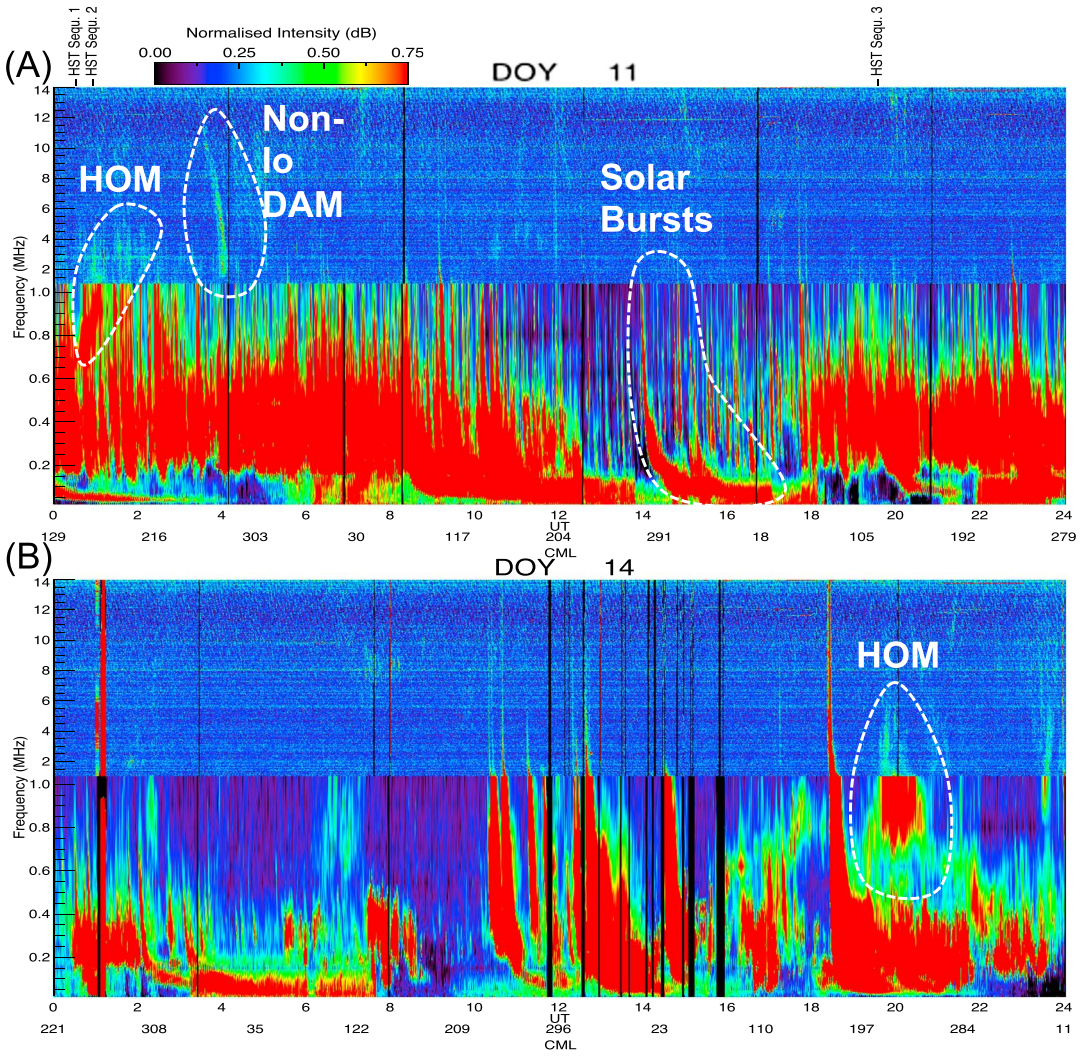

Figure 6. Radio spectra from Wind/WAVES RAD1 (20–1040 kHz) and RAD2(1.075–13.82 MHz) detectors on (a) day 11 and (b) day 14. The flux density of both receivers is not cross calibrated, producing the apparent discontinuity across the detector ranges. HOM emission is expected up to a few MHz. The HOM emission on day 11 is the between ~00:30–02:30 UT and 150–220° CML, between 0.8 and 4 MHz. The HST image sequences are marked for indication: HST Sequence 1 (00:31–00:41 UT), HST Sequence 2 (01:01–01:11 UT), and the next sequence showing the relaxed main emission state, HST Sequence 3 (19:39–19:49 UT). A clearer HOM signal for comparison on day 14 is between ~19:30–21:00 UT and 205–265° CML, between 0.7 and 6 MHz. The non-Io DAM signature on day 11 is at ~04:00 UT and ~ 270° CML. A typical solar burst showing decreasing frequency with time is highlighted. The color scale is saturated at 1.5 dB to show type III solar bursts.

simultaneously with the intense UV emission observed by HST (Figures 1b–1e). The specific UV auroral feature that the HOM corresponds to is unknown, although HOM is expected to be related to inner magnetospheric sources (L shell < 30) [*Ladreiter et al.*, 1994; *Zarka et al.*, 2001; *Imai et al.*, 2015]. Figure 3 shows part of the main emission and equatorward emissions relate to sources up to L ~30.

For comparison, in Figure 6b we show another HOM burst from 19:30 to 21:00 UT between 205 and 265° CML on day 14, which was also correlated with intense UV emission [*Kimura et al.*, 2015]. Because of its higher power this feature is easier to distinguish on the frequency-time spectrogram, but otherwise, its characteristics are similar to those seen at 00:30–02:30 UT on day 11, supporting our interpretation of the day 11 feature as a HOM burst associated with enhanced UV emission.

Non-Io DAM emission was also observed at 04 UT, CML 275° at 1–10 MHz. The vertex-late shape corresponds to a dusk source [*Hess et al.*, 2014]. At this time, approximately one fourth rotation after the images shown in Figures 1b–1e, the bright main emission feature B and equatorward feature C would be in the dusk and postdusk sectors, assuming corotation with the planet. *Hess et al.* [2014] suggest that DAM sometimes exhibits

a correlation with solar wind shocks, as has been detected in the UV [*Clarke et al.*, 2009; *Nichols et al.*, 2009]. However, within ~1 day accuracy, there is no evidence in the propagated SW data of a SW shock arriving at Jupiter at this time [*Tao et al.*, 2016]. This could therefore be an internally triggered DAM emission, as identified by *Hess et al.* [2012, 2014].

The intensifications of the emissions identified as HOM and DAM support the interpretation that a global magnetospheric disturbance was occurring, involving tail reconnection and disturbance of the outer Io plasma torus [*Louarn et al.*, 2014]. The large equatorward emissions are thought to be generated by inflows prior to the HOM detection and HST imaging sequence on day 11. This implies that there has been magnetotail reconnection prior to the time of the HST observations. This could be analogous to Saturn Kilometric Radiation (SKR) and auroral UV enhancements and large scale plasma injections at Saturn [e.g., *Mitchell et al.*, 2009; *Lamy et al.*, 2013].

5. Conclusion and Summary

HST observations from day 11 January 2014 (01:01–01:11 UT) show bright and unusual auroral forms, which are interpreted as part of an inward radial transport sequence. A superrotating polar dawn spot (feature A) was observed and interpreted as the signature of tail reconnection. The spot could be either the signature of the propagation of the X line in the tail or the signature of dipolarized field traveling planetward. The spot was observed to move into a broad and bright patch along the dawnside main emission (B). The brightening in this region could be related to flow shears associated with earlier inflows. The presence of hot plasma originating from the tail could lead to the presence of bright equatorward emissions (C and D) as the signatures of earlier hot plasma injections [e.g., *Thomsen et al.*, 2015]. The images are thought to capture part of a prolonged period of reconnection.

Radio emissions measured by Wind suggest that HOM and non-Io DAM signatures are associated with the sequence of auroral signatures (01:01–01:11 UT). These are interpreted as inner magnetospheric and internally driven disturbances. *Louarn et al.* [2014] previously showed HOM should occur within 10 h of tail inflows. The enhancement/detection of the HOM supports our interpretation of the UV auroral signatures as a sequence of radial transport.

The bright and broad dawnside main emission feature magnetically maps to the morphological boundary between the hot tail inflows and inner magnetosphere region. The Hisaki EUV power is only elevated for about 7 h above the average power level, so assuming the main contributor to the EUV power is the main emission feature, the lifetime of feature B may be constrained to just ~7 h. If flow shears in the middle magnetosphere are the cause of the emission, then the flow shears and therefore the enhanced inflow may also be constrained to a duration of 7 h. The equatorward images may show emission for at least 18.5 h. This implies the interval of hot plasma injections and its consequences can be at least 18.5 h duration.

Long-term monitoring could have indicated the state of the system prior to and further through day 11, allowing investigation of the interface between the superrotating spot and the main emission. We therefore look forward to polar science orbits of Juno, from which the timescale of reconnection flows to transition to the inner magnetosphere could be determined.

Acknowledgments
R.L.G. was supported by a STFC studentship. S.V.B. was supported by an RAS fellowship and an STFC Ernest Rutherford Fellowship. J.D.N. was supported by an STFC Advanced Fellowship (ST/I004084/1). M.F.V. was supported by the National Science Foundation under award 1524651. B.B. was supported by the PRODEX program managed by ESA in collaboration with the Belgian Federal Science Policy Office. L.C.R. was supported by an STFC consolidated grant (ST/N000722/1). This work is based on observations made with the NASA/ESA Hubble Space Telescope (observation ID: GO13035), obtained at the Space Telescope Science Institute (STScI), which is operated by AURA, Inc., for NASA. The Hubble observations are available from the STScI website. The authors would like to acknowledge the contributions of teams involved in the Wind spacecraft mission, NASA. The Wind/WAVES data are available through CDAWeb.

References

Badman, S. V., and S. W. H. Cowley (2007), Significance of Dungey-cycle flows in Jupiter's and Saturn's magnetospheres, and their identification on closed equatorial field lines, *Ann. Geophys.*, *25*, 941–951, doi:10.5194/angeo-25-941-2007.

Badman, S. V., et al. (2016), Weakening of Jupiter's main auroral emission during January 2014, *Geophys. Res. Lett.*, *43*, 988–997, doi:10.1002/2015GL067366.

Bonfond, B. (2012), When moons create aurora: The satellite footprints on giant planets, in *Auroral Phenomenology and Magnetospheric Processes: Earth and Other Planets, Geophys. Monogr. Ser.*, vol. 197, edited by A. Keiling et al., pp. 133–140, AGU, Washington, D. C., doi:10.1029/2011GM001169.

Bonfond, B., D. Grodent, J.-C. Gérard, T. Stallard, J. T. Clarke, M. Yoneda, A. Radioti, and J. Gustin (2012), Auroral evidence of Io's control over the magnetosphere of Jupiter, *Geophys. Res. Lett.*, *39*, L01105, doi:10.1029/2011GL050253.

Bougeret, J.-L., et al. (1995), Waves: The radio and plasma wave investigation on the wind spacecraft, *Space Sci. Rev.*, *71*(1–4), 231–263.

Clarke, J. T., H. W. Moos, S. K. Atreya, and A. L. Lane (1980), Observations from earth orbit and variability of the polar aurora on Jupiter, *Astrophys. J. Lett.*, *241*, L179–L182, doi:10.1086/183386.

Clarke, J. T., et al. (2009), Response of Jupiter's and Saturn's auroral activity to the solar wind, *J. Geophys. Res.*, *114*, A05210, doi:10.1029/2008JA013694.

Cowley, S. W. H., and E. J. Bunce (2001), Origin of the main auroral oval in Jupiter's coupled magnetosphere-ionosphere system, *Planet. Space. Sci.*, *49*, 1067–1088, doi:10.1016/S0032-0633(00)00167-7.

Cowley, S. W. H., J. D. Nichols, and C. M. Jackman (2015), Down-tail mass loss by plasmoids in Jupiter's and Saturn's magnetospheres, *J. Geophys. Res. Space Physics*, *120*, 6347–6356, doi:10.1002/2015JA021500.

Dessler, A. J. (1983), *Physics of the Jovian Magnetosphere*, Cambridge Univ. Press, Cambridge, U. K.

Dumont, M., D. Grodent, A. Radioti, and J.-C. Gérard (2014), Jupiter's equatorward auroral features: Possible signatures of magnetospheric injections, *J. Geophys. Res. Space Physics*, *119*, 10,068–10,077, doi:10.1002/2014JA020527.

Galopeau, P. H. M., and M. Y. Boudjada (2005), Solar wind control of Jovian auroral emissions, *J. Geophys. Res.*, *110*, A09221, doi:10.1029/2004JA010843.

Ge, Y., C. Russell, and K. Khurana (2010), Reconnection sites in Jupiter's magnetotail and relation to Jovian auroras, *Planet. Space Sci.*, *58*(11), 1455–1469.

Gladstone, G. R., et al. (2002), A pulsating auroral X-ray hot spot on Jupiter, *Nature*, *415*, 1000–1003.

Grodent, D., J. T. Clarke, J. Kim, J. H. Waite, and S. W. H. Cowley (2003), Jupiter's main auroral oval observed with HST-STIS, *J. Geophys. Res.*, *108*(A11), 1389, doi:10.1029/2003JA009921.

Grodent, D., J.-C. Gérard, J. T. Clarke, G. R. Gladstone, and J. H. Waite (2004), A possible auroral signature of a magnetotail reconnection process on Jupiter, *J. Geophys. Res.*, *109*, A05201, doi:10.1029/2003JA010341.

Grodent, D., B. Bonfond, J.-C. Gérard, A. Radioti, J. Gustin, J. T. Clarke, J. Nichols, and J. E. P. Connerney (2008), Auroral evidence of a localized magnetic anomaly in Jupiter's northern hemisphere, *J. Geophys. Res.*, *113*, A09201, doi:10.1029/2008JA013185.

Gurnett, D. A., et al. (2002), Control of Jupiter's radio emission and aurorae by the solar wind, *Nature*, *415*, 985–987.

Gustin, J., J.-C. Gérard, G. R. Gladstone, D. Grodent, and J. T. Clarke (2006), Characteristics of Jovian morning bright FUV aurora from Hubble Space Telescope/Space Telescope Imaging Spectrograph imaging and spectral observations, *J. Geophys. Res.*, *111*, A09220, doi:10.1029/2006JA011730.

Gustin, J., B. Bonfond, D. Grodent, and J.-C. Gérard (2012), Conversion from HST ACS and STIS auroral counts into brightness, precipitated power, and radiated power for H_2 giant planets, *J. Geophys. Res.*, *117*, A07316, doi:10.1029/2012JA017607.

Henderson, M. G., G. D. Reeves, and J. S. Murphree (1998), Are north-south aligned auroral structures an ionospheric manifestation of bursty bulk flows?, *Geophys. Res. Lett.*, *25*(19), 3737–3740, doi:10.1029/98GL02692.

Hess, S. L. G., B. Bonfond, P. Zarka, and D. Grodent (2011), Model of the Jovian magnetic field topology constrained by the Io auroral emissions, *J. Geophys. Res.*, *116*, A05217, doi:10.1029/2010JA016262.

Hess, S. L. G., E. Echer, and P. Zarka (2012), Solar wind pressure effects on Jupiter decametric radio emissions independent of Io, *Planet. Space. Sci.*, *70*, 114–125, doi:10.1016/j.pss.2012.05.011.

Hess, S. L. G., E. Echer, P. Zarka, L. Lamy, and P. Delamere (2014), Multi-instrument study of the Jovian radio emissions triggered by solar wind shocks and inferred magnetospheric subcorotation rates, *Planet. Space. Sci.*, *99*, 136–148.

Hill, T. W. (2001), The Jovian auroral oval, *J. Geophys. Res.*, *106*, 8101–8108, doi:10.1029/2000JA000302.

Imai, M., A. Lecacheux, M. Moncuquet, F. Bagenal, C. A. Higgins, K. Imai, and J. R. Thieman (2015), Modeling Jovian hectometric attenuation lanes during the Cassini flyby of Jupiter, *J. Geophys. Res. Space Physics*, *120*, 1888–1907, doi:10.1002/2014JA020815.

Joy, S. P., M. G. Kivelson, R. J. Walker, K. K. Khurana, C. T. Russell, and T. Ogino (2002), Probabilistic models of the Jovian magnetopause and bow shock locations, *J. Geophys. Res.*, *107*, 1309, doi:10.1029/2001JA009146.

Kasahara, S., E. A. Kronberg, N. Krupp, T. Kimura, C. Tao, S. V. Badman, A. Retinò, and M. Fujimoto (2011), Magnetic reconnection in the Jovian tail: X-line evolution and consequent plasma sheet structures, *J. Geophys. Res.*, *116*, A11219, doi:10.1029/2011JA016892.

Kasahara, S., E. A. Kronberg, T. Kimura, C. Tao, S. V. Badman, A. Masters, A. Retinò, N. Krupp, and M. Fujimoto (2013), Asymmetric distribution of reconnection jet fronts in the Jovian nightside magnetosphere, *J. Geophys. Res. Space Physics*, *118*, 375–384.

Keiling, A., et al. (2009), Substorm current wedge driven by plasma flow vortices: THEMIS observations, *J. Geophys. Res.*, *114*, A00C22, doi:10.1029/2009JA014114.

Kimura, T., et al. (2015), Transient internally-driven aurora at Jupiter discovered by Hisaki and the Hubble Space Telescope, *Geophys. Res. Lett.*, *42*, 1662–1668, doi:10.1002/2015GL063272.

Kivelson, M. G., and K. K. Khurana (2002), Properties of the magnetic field in the Jovian magnetotail, *J. Geophys. Res.*, *107*(A8), 1196, doi:10.1029/2001JA000249.

Kivelson, M. G., K. K. Khurana, C. T. Russell, and R. J. Walker (1997), Intermittent short-duration magnetic field anomalies in the Io torus: Evidence for plasma interchange?, *Geophys. Res. Lett.*, *24*(17), 2127–2130, doi:10.1029/97GL02202.

Kronberg, E. A., J. Woch, N. Krupp, A. Lagg, K. K. Khurana, and K.-H. Glassmeier (2005), Mass release at Jupiter: Substorm-like processes in the Jovian magnetotail, *J. Geophys. Res.*, *110*, A03211, doi:10.1029/2004JA010777.

Krupp, N., et al. (2004), Dynamics of the Jovian magnetosphere, in *Jupiter: The Planet, Satellites and Magnetosphere*, edited by F. Bagenal et al., pp. 617–638, Cambridge Univ. Press, Cambridge, U. K.

Ladreiter, H. P., P. Zarka, and A. Lacacheux (1994), Direction finding study of Jovian hectometric and broadband kilometric radio emissions: Evidence for their auroral origin, *Planet. Space. Sci.*, *42*, 919–931, doi:10.1016/0032-0633(94)90052-3.

Lamy, L., R. Prangé, W. Pryor, J. Gustin, S. V. Badman, H. Melin, T. Stallard, D. G. Mitchell, and P. C. Brandt (2013), Multi-spectral simultaneous diagnosis of Saturn's aurorae throughout a planetary rotation, *J. Geophys. Res. Space Physics*, *118*, 4817–4843, doi:10.1002/jgra.50404.

Louarn, P., C. P. Paranicas, and W. S. Kurth (2014), Global magnetodisk disturbances and energetic particle injections at Jupiter, *J. Geophys. Res. Space Physics*, *119*, 4495–4511, doi:10.1002/2014JA019846.

Mauk, B. H., D. J. Williams, R. W. McEntire, K. K. Khurana, and J. G. Roederer (1999), Storm-like dynamics of Jupiter's inner and middle magnetosphere, *J. Geophys. Res.*, *104*, 22,759–22,778, doi:10.1029/1999JA900097.

Mauk, B. H., J. T. Clarke, D. Grodent, J. H. Waite, C. P. Paranicas, and D. J. Williams (2002), Transient aurora on Jupiter from injections of magnetospheric electrons, *Nature*, *415*, 1003–1005.

Mitchell, D. G., et al. (2009), Recurrent energization of plasma in the midnight-to-dawn quadrant of Saturn's magnetosphere, and its relationship to auroral UV and radio emissions, *Planet. Space. Sci.*, *57*, 1732–1742, doi:10.1016/j.pss.2009.04.002.

Mitchell, D. G., et al. (2015), *Injection, Interchange, and Reconnection*, John Wiley, pp. 327–343, Hoboken, N. J.

Nakamura, R., W. Baumjohann, R. Schödel, M. Brittnacher, V. A. Sergeev, M. Kubyshkina, T. Mukai, and K. Liou (2001), Earthward flow bursts, auroral streamers, and small expansions, *J. Geophys. Res.*, *106*(A6), 10,791–10,802, doi:10.1029/2000JA000306.

Nichols, J., and S. Cowley (2004), Magnetosphere-ionosphere coupling currents in Jupiter's middle magnetosphere: Effect of precipitation-induced enhancement of the ionospheric Pedersen conductivity, *Ann. Geophys.*, *22*, 1799–1827, doi:10.5194/angeo-22-1799-2004.

Nichols, J. D. (2011), Magnetosphere-ionosphere coupling in Jupiter's middle magnetosphere: Computations including a self-consistent current sheet magnetic field model, *J. Geophys. Res.*, *116*, A10232, doi:10.1029/2011JA016922.

Nichols, J. D., and S. W. H. Cowley (2003), Magnetosphere-ionosphere coupling currents in Jupiter's middle magnetosphere: Dependence on the effective ionospheric Pedersen conductivity and iogenic plasma mass outflow rate, *Ann. Geophys.*, *21*, 1419–1441, doi:10.5194/angeo-21-1419-2003.

Nichols, J. D., J. T. Clarke, J. C. Gérard, D. Grodent, and K. C. Hansen (2009), Variation of different components of Jupiter's auroral emission, *J. Geophys. Res.*, *114*, A06210, doi:10.1029/2009JA014051.

Nichols, J. D., et al. (2014), Dynamic auroral storms on Saturn as observed by the Hubble Space Telescope, *Geophys. Res. Lett.*, *41*, 3323–3330, doi:10.1002/2014GL060186.

Nishimura, Y., L. R. Lyons, V. Angelopoulos, T. Kikuchi, S. Zou, and S. B. Mende (2011), Relations between multiple auroral streamers, pre-onset thin arc formation, and substorm auroral onset, *J. Geophys. Res.*, *116*, A09214, doi:10.1029/2011JA016768.

Pallier, L., and R. Prangé (2001), More about the structure of the high latitude Jovian aurorae, *Planet. Space Sci.*, *49*, 1159–1173, doi:10.1016/S0032-0633(01)00023-X.

Palmaerts, B., A. Radioti, D. Grodent, E. Chané, and B. Bonfond (2014), Transient small-scale structure in the main auroral emission at Jupiter, *J. Geophys. Res. Space Physics*, *119*, 9931–9938, doi:10.1002/2014JA020688.

Radioti, A., D. Grodent, J.-C. Gérard, B. Bonfond, and J. T. Clarke (2008), Auroral polar dawn spots: Signatures of internally driven reconnection processes at Jupiter's magnetotail, *Geophys. Res. Lett.*, *35*, L03104, doi:10.1029/2007GL032460.

Radioti, A., A. T. Tomás, D. Grodent, J.-C. Gérard, J. Gustin, B. Bonford, N. Krupp, J. Woch, and J. D. Menietti (2009), Equatorward diffuse auroral emissions at Jupiter: Simultaneous HST and Galileo observations, *Geophys. Res. Lett.*, *36*, L07101, doi:10.1029/2009GL037857.

Radioti, A., D. Grodent, J.-C. Gérard, and B. Bonfond (2010), Auroral signatures of flow bursts released during magnetotail reconnection at Jupiter, *J. Geophys. Res.*, *115*, A07214, doi:10.1029/2009JA014844.

Radioti, A., D. Grodent, J.-C. Gérard, M. F. Vogt, M. Lystrup, and B. Bonfond (2011), Nightside reconnection at Jupiter: Auroral and magnetic field observations from 26 July 1998, *J. Geophys. Res.*, *116*, A03221, doi:10.1029/2010JA016200.

Ray, L. C., R. E. Ergun, P. A. Delamere, and F. Bagenal (2012), Magnetosphere-ionosphere coupling at Jupiter: A parameter space study, *J. Geophys. Res.*, *117*, A01205, doi:10.1029/2011JA016899.

Tao, C., T. Kimura, S. V. Badman, N. André, F. Tsuchiya, G. Murakami, K. Yoshioka, I. Yoshikawa, A. Yamazaki, and M. Fujimoto (2016), Variation of Jupiter's aurora observed by Hisaki/EXCEED: 2. Estimations of auroral parameters and magnetospheric dynamics, *J. Geophys. Res. Space Physics*, *121*, 4055–4071, doi:10.1002/2015JA021272.

Thomsen, M. F., D. G. Mitchell, X. Jia, C. M. Jackman, G. Hospodarsky, and A. J. Coates (2015), Plasmapause formation at Saturn, *J. Geophys. Res. Space Physics*, *120*, 2571–2583, doi:10.1002/2015JA021008.

Thorne, R. M., T. P. Armstrong, S. Stone, D. J. Williams, R. W. McEntire, S. J. Bolton, D. A. Gurnett, and M. G. Kivelson (1997), Galileo evidence for rapid interchange transport in the Io torus, *Geophys. Res. Lett.*, *24*, 2131–2134, doi:10.1029/97GL01788.

Tomás, A., J. Woch, N. Krupp, A. Lagg, K.-H. Glassmeier, M. K. Dougherty, and P. G. Hanlon (2004), Changes of the energetic particles characteristics in the inner part of the Jovian magnetosphere: A topological study, *Planet. Space. Sci.*, *52*, 491–498, doi:10.1016/j.pss.2003.06.011.

Tomás, A. T., J. Woch, N. Krupp, A. Lagg, K.-H. Glassmeier, and W. S. Kurth (2004), Energetic electrons in the inner part of the Jovian magnetosphere and their relation to auroral emissions, *J. Geophys. Res.*, *109*, A06203, doi:10.1029/2004JA010405.

Tsuchiya, F., et al. (2015), Local electron heating in Io plasma torus associated with Io from Hisaki satellite observation, *J. Geophys. Res. Space Physics*, *120*, 10,317–10,333, doi:10.1002/2015JA021420.

Vasavada, A. R., A. H. Bouchez, A. P. Ingersoll, B. Little, C. D. Anger, and G. S. Team (1999), Jupiter's visible aurora and Io footprint, *J. Geophys. Res.*, *104*, 27,133–27,142, doi:10.1029/1999JE001055.

Vasyliunas, V. M. (1983), Plasma distribution and flow, in *Physics of the Jovian Magnetosphere*, edited by V. M. Vasyliunas, pp. 395–453, Cambridge Univ. Press, Cambridge and New York.

Vogt, M. F., M. G. Kivelson, K. K. Khurana, S. P. Joy, and R. J. Walker (2010), Reconnection and flows in the Jovian magnetotail as inferred from magnetometer observations, *J. Geophys. Res.*, *115*, A06219, doi:10.1029/2009JA015098.

Vogt, M. F., M. G. Kivelson, K. K. Khurana, R. J. Walker, B. Bonfond, D. Grodent, and A. Radioti (2011), Improved mapping of Jupiter's auroral features to magnetospheric sources, *J. Geophys. Res.*, *116*, A03220, doi:10.1029/2010JA016148.

Vogt, M. F., C. M. Jackman, J. A. Slavin, E. J. Bunce, S. W. H. Cowley, M. G. Kivelson, and K. K. Khurana (2014), Structure and statistical properties of plasmoids in Jupiter's magnetotail, *J. Geophys. Res. Space Physics*, *119*, 821–843, doi:10.1002/2013JA019393.

Vogt, M. F., E. J. Bunce, M. G. Kivelson, K. K. Khurana, R. J. Walker, A. Radioti, B. Bonfond, and D. Grodent (2015), Magnetosphere-ionosphere mapping at Jupiter: Quantifying the effects of using different internal field models, *J. Geophys. Res. Space Physics*, *120*, 2584–2599, doi:10.1002/2014JA020729.

Woodfield, E. E., R. B. Horne, S. A. Glauert, J. D. Menietti, and Y. Y. Shprits (2013), Electron acceleration at Jupiter: Input from cyclotron-resonant interaction with whistler-mode chorus waves, *Ann. Geophys.*, *31*(10), 1619–1630, doi:10.5194/angeo-31-1619-2013.

Yoneda, M., F. Tsuchiya, H. Misawa, B. Bonfond, C. Tao, M. Kagitani, and S. Okano (2013), Io's volcanism controls Jupiter's radio emissions, *Geophys. Res. Lett.*, *40*, 671–675, doi:10.1002/grl.50095.

Yoneda, M., M. Kagitani, F. Tsuchiya, T. Sakanoi, and S. Okano (2015), Brightening event seen in observations of Jupiter's extended sodium nebula, *Icarus*, *261*, 31–33, doi:10.1016/j.icarus.2015.07.037.

Zarka, P., J. Queinnec, and F. J. Crary (2001), Low-frequency limit of Jovian radio emissions and implications on source locations and Io plasma wake, *Planet. Space Sci.*, *49*(10–11), 1137–1149, doi:10.1016/S0032-0633(01)00021-6.